

DNA Binding to Protein–Gold Nanocrystal Conjugates

Michelle K. Calabretta,^{§,*} Kathleen S. Matthews,[†] and Vicki L. Colvin[§]

Department of Chemistry and Department of Biochemistry and Cell Biology, Rice University, 6100 Main Street, Houston, Texas 77005. Received April 9, 2006; Revised Manuscript Received June 1, 2006

The *E. coli* DNA binding protein *lac* repressor (LacI) and a derivative with a designed thiol (T334C) were developed as gold nanocrystal conjugates to assess the effects of conjugation on DNA binding function. The designed derivative was engineered with a solvent-accessible thiol to promote oriented conjugation, avoiding obstruction of the DNA-binding domain by the nanocrystal. Analytical ultracentrifugation (AU) and electrophoretic mobility shift assays (EMSA) were used to evaluate the ability of conjugated repressors to bind the natural operator DNA sequence O¹. The results show that LacI does not retain significant DNA binding function when conjugated to gold nanocrystals, presumably because the basic DNA-binding domain is the site for nonspecific conjugation. T334C, with the potential for both directed and nonspecific conjugation, shows enhanced interaction with O¹ when conjugated. Interestingly, the order of component addition is a key factor in producing functional *lac* repressor conjugates.

INTRODUCTION

DNA recognition proteins have recently been the subject of interest in nanoscience (1–5). Yun and co-workers (2002) tested the ability of DNA binding proteins to interact with DNA oligonucleotides tethered on both ends to small (1.4 nm) gold nanocrystals. Interparticle distances obtained from TEM demonstrate that EcoRI can cause topological changes, such as bending, in conjugated DNA. This type of manipulation generates the potential for design of nanoarchitectures for electronics and sensors (5). Protein–DNA complexes have also been used as functional scaffolds for the fabrication of nanoelectronics. For example, Keren and co-workers used the structural and functional properties of the RecA nucleoprotein filament to produce gold nanowires with branched architectures and other structural characteristics (1). Another nanoarchitecture, using protruding biotinylated thymine loops on DNA oligonucleotides, produced uniformly spaced streptavidin-coated gold nanocrystals. The researchers propose that regularly spaced arrays of gold nanocrystals could interconnect nanoelectronic components and aid in the development of logical nanoelectronic devices (2).

The *lac* repressor (LacI), an *E. coli* DNA binding protein, is attractive for use as a structural and functional nano building block because of the large amount of genetic and biochemical information available for this protein (for review see ref 6). LacI is structurally well characterized, with several crystallographic and solution structures available. This protein binds two types of ligand: DNA (operator) and small sugar molecules (inducer). The binding of an inducer sugar reduces the ability of LacI to bind DNA, effectively making LacI a logic switch, where “on” is the high DNA affinity state and “off” is in the presence of inducer when DNA affinity is low. One approach to the assembly of nanoelectronic components onto DNA nanostructures could utilize the specificity of DNA binding proteins, like LacI, for their DNA substrates. For example, DNA sequences created with natural operator sequence O¹ at regular intervals could be mixed with LacI-bound gold nanocrystals, resulting in uniformly spaced gold nanocrystal architectures. This type

of application requires oriented protein conjugation and would be sensitive to the ability of the conjugated repressor to interact with DNA, which is in turn modulated by inducer binding.

There is substantial evidence that nonspecific protein–gold nanocrystal interactions are largely electrostatic, occurring through basic surface residues and the negatively charged nanocrystal surface (7, 8). The DNA-binding domain is logically the most probable region for gold nanocrystal conjugation to LacI because it is highly basic, having a theoretical pI ~9.3, and lacks well-defined structure in the absence of operator DNA, providing easy accessibility (9). If the DNA-binding domain is the site of interaction, then LacI–gold nanocrystal conjugates would be sterically prevented from binding operator DNA. The purpose for creating T334C, with its solvent accessible cysteines, was to provide a means for thiol-directed conjugation to gold through the C-terminal region of LacI, thereby precluding nanocrystal interference with the DNA-binding domain. Here, we assess the operator DNA binding affinity of LacI and T334C gold nanocrystal conjugates. This work develops the understanding of how conjugation can be manipulated to optimize the function of protein–nanocrystal materials.

EXPERIMENTAL PROCEDURES

Materials. All materials were purchased from Sigma unless specified otherwise.

Protein Mutation, Purification, and Conjugation. The T334C mutation was produced on plasmid pLS1 (10) with the QuikChange PCR site-directed mutagenesis kit (Stratagene) using the provided protocol. Mutant plasmids were transformed into supercompetent GC5 cells (Gene Choice) for growth and purification. Mutant plasmids were sequenced (SeqWright) to verify that no other mutations were present. Purification of wild type LacI was carried out as described previously (11–14). Briefly, expression occurred in *E. coli* strain BLIM (Novagen), which was cured of the LacI episome (15). After centrifugation, cell culture pellets were resuspended and lysed, and the lysis supernatant was precipitated in 37% ammonium sulfate. The resuspended precipitate was dialyzed overnight and loaded onto phosphocellulose. LacI was eluted with a gradient of 0.12–0.3 M potassium phosphate buffer, pH 7.5. The concentration of LacI-containing fractions was determined by absorbance at 280 nm (extinction coefficient = 1.6 mL mg⁻¹ cm⁻¹). The T334C

* Corresponding author. Phone: (713)348-4936; E-mail: mcal@rice.edu.

§ Department of Chemistry.

† Department of Biochemistry and Cell Biology.

mutant was purified similarly to wild type protein, with the following exceptions: Protease inhibitor tabs (Roche) were added to inhibit degradation of the protein. Dialysis time of the resuspended ammonium sulfate pellet is reduced to three 20-min steps. All buffers contained 10 mM DTT to prevent aggregation via the solvent-exposed cysteine residues. Last, T334C was eluted stepwise (0.12 M KP to 0.3 M KP) instead of with a gradient to minimize time of purification. Proteins were stored at $-20\text{ }^{\circ}\text{C}$ for up to 6 months with 10 mM DTT.

Conjugates were formed as follows: The LacI potassium phosphate storage buffer was exchanged for conjugation buffer (50 mM Tris, pH 9.2, 5% (w/v) glucose) by centrifugation in Amicon Ultra-15 (MWCO 30000) centrifugal filters (Millipore). LacI or T334C (250 μL) was diluted into 15 mL of conjugation buffer and centrifuged at 2500g for 15 min. The process was repeated twice more to ensure complete exchange. A gold nanocrystal suspension, prepared by citrate reduction and characterized as described previously (14), was added to specified repressor concentrations diluted in conjugation buffer so that the final concentration of gold nanocrystal was one-fourth the initial concentration. This dilution factor was necessary to decrease the nanocrystal absorbance in the UV–visible region to below 1 absorbance unit and sufficiently dilutes the nanocrystals so that concentration-dependent nonideality in sedimentation is minimized. Samples were allowed to conjugate for approximately 30 min at room temperature unless specified otherwise.

[^{35}S]-Methionine-labeled LacI and T334C were generated as described previously (14) with the TNT T7 Quick for PCR DNA transcription/translation kit (Promega). Briefly, the LacI gene (with and without the T334C mutation) under the T7 promoter was cloned into pGEM-T (Promega). Following translation, unincorporated [^{35}S]-methionine (ICON Isotopes) was removed with protein desalting spin columns (Pierce). [^{35}S]-repressors were further purified on a small phosphocellulose column and diluted with unlabeled repressor to determine protein concentration ($\mu\text{g}/\mu\text{L}$) by absorbance at 280 nm. The amount of radioactive isotope in counts per minute (cpm) was measured for an aliquot of the repressor mixture to produce a specific activity (cpm/g) for the sample. For [^{35}S]-repressor–gold nanocrystal conjugates, free protein was removed by centrifugation at 14000 rpm for 30 min in a desktop centrifuge. The conjugated repressor concentration was determined based on the amount of radioactive isotope present using the specific activity of the initial protein sample.

Operator DNA Radiolabeling. Operator affinities of conjugated proteins were measured with double-stranded natural operator O¹ (5'-TGTTGTGTGGAATTGTGAGCGGATAACAATTTCACACAGG-3'). Complementary strands (BioSource) were hybridized in annealing buffer (8 mM Tris-HCl, pH 7.5, 4 mM MgCl₂, 10 mM NaCl) and labeled with [^{32}P] by polynucleotide kinase (NEB) and γ -[^{32}P]-ATP (MP Biomedicals) in a final volume of 15 μL . The labeling reaction was terminated with 2 μL of 0.5 M EDTA and diluted to 50 μL with Tris-EDTA, pH 8. Labeled operator was purified from unincorporated γ -[^{32}P]-ATP on NICK columns (Amersham Biosciences) and eluted with Tris-EDTA, pH 8.0. DNA was aliquoted and stored at $-20\text{ }^{\circ}\text{C}$ for up to 1 month.

Analytical Ultracentrifugation (AU). AU data were collected using the vendor's software on a Beckman XL-A analytical ultracentrifuge. Sedimentation velocity experiments were performed at 20 $^{\circ}\text{C}$ at 3100 rpm. A total of 80 scans were taken at 10 scans per hour for each sample. Raw data were processed with the enhanced van Holde–Weischet and second moment utilities in Ultrascan version 7.2 (16).

NaCl Flocculation Assays. Conjugates, prepared as described above, were mixed with NaCl to a final concentration of 1%. Flocculation proceeded for 10 min before recording the UV–

visible spectra (200–800 nm) on a Varian Cary 50 UV–visible spectrophotometer. A minimum of three spectra for each protein concentration were recorded.

Electrophoretic Mobility Shift Assay (EMSA). Nondenaturing 4% polyacrylamide (37.5:1 acrylamide:bisacrylamide) gels containing 2% glycerol were preelectrophoresed in 0.5 \times TBE (0.045 M Tris-borate, pH 8.0, 1.0 mM EDTA) at 100 V, constant current, for 1 h prior to loading the samples. Conjugate-[^{32}P]-O¹ interactions were measured in conjugation buffer at pH 8 (50 mM Tris-HCl, pH 8, 5% glucose w/v), with BSA added to a final concentration of 1 mg/mL just prior to loading to aid in entry of the sample into the gel. Samples were loaded onto gels at 250 V until separation of loading dye occurred. The voltage was reduced to 150 V, and gels were run for approximately 1.5 h or until the loading dye reached a distance of 6 cm into the gel. Gels were dried with a vacuum gel dryer and exposed overnight to a Fuji phosphorimaging plate. Binding data were visualized and quantified with MultiGauge software (Fuji).

RESULTS

The DNA recognition capability of LacI requires contact between operator DNA (O¹) and the charged binding domain of LacI. Negatively charged gold nanocrystals could in principle interact with this important region and render the protein inactive. With that possibility in mind, we developed a mutant of LacI, T334C, to direct nanocrystal attachment to another region of the protein. This system contains a solvent-exposed cysteine residue in the C-terminus, on the opposite end of the protein from the N-terminal DNA-binding domain. Figure 1 shows the crystal structure of tetrameric LacI and the position of the basic DNA-binding domain and threonine 334 on each monomer. The cysteine mutation provides potential for site-directed conjugation via a gold–sulfur bond, and its location would orient the DNA-binding domain away from the nanocrystal. Additionally, nanocrystal attachment to the cysteines of T334C would require a stronger, more stable gold–sulfur bond than the nonspecific and reversible electrostatic interactions expected for binding between gold nanocrystals and the native LacI repressor (17).

Central to any comparison of function between nanoparticle-bound and free proteins is accurate evaluation of the stoichiometry of the nanobionconjugates; in particular, it is important that nanobioconjugates are produced with saturation coverage of proteins and that free protein is removed from the suspensions. Here, these issues were addressed for gold nanocrystal–repressor conjugates using three methods: NaCl-induced flocculation, [^{35}S]-repressor association, and analytical ultracentrifugation. Taken together these techniques provide both a measure of the success of conjugation strategies, and also a determination of the stoichiometry of the resulting complexes. The results from all methods are summarized in Table 1.

In NaCl-induced flocculation assays, gold nanocrystals become aggregated because of the reduced electrostatic repulsion at higher ionic strengths. This aggregation is signaled by a pronounced shift in the peak position of their absorbance. If nanocrystals are bound to proteins, the aggregation is modified significantly and can in fact be avoided when nanocrystals are fully coated by proteins. Thus, an examination of the gold nanocrystal–repressor solutions as a function of [gold nanocrystal]/[repressor] ratio provides a verification of the successful conjugation of LacI and T334C to nanocrystals. Figure 2 shows that ~ 12 LacI repressors are needed to prevent flocculation, whereas a smaller number of repressors produce the same outcome for T334C (Table 1). These data suggest that reversible electrostatic interactions are important in the conjugation of gold nanocrystals to the native LacI repressor. Compared to a stronger

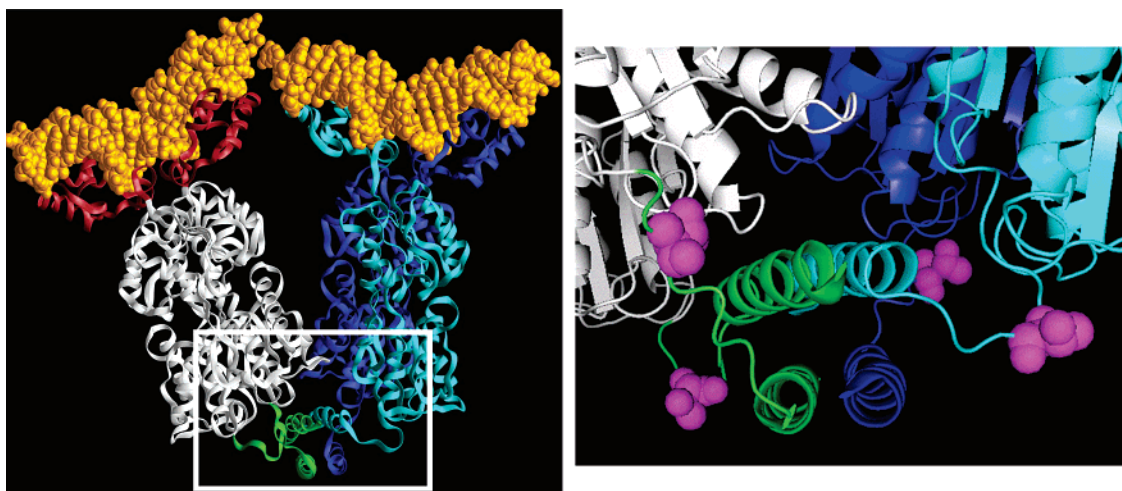


Figure 1. Crystal structure of LacI and placement of the T334C mutation. LacI is a dimer of dimers. In the right dimer, one monomer of LacI is shown in light blue and the other in dark blue. In the left dimer, the DNA-binding domain is colored red, the core domain (that binds sugar inducer) of the protein white, and the tetramerization domain in green. Operator DNA is shown as the yellow space-filled molecule. The white box indicates the region for enlargement to show the position of threonine 334. Threonine 334, shown in magenta in the enlargement, was chosen for cysteine mutation because it is solvent accessible and should orient the protein so that neither the DNA-binding domain nor the inducer sugar pocket are obstructed when the protein is bound to gold nanocrystals. Figure generated from pdb files 1LBI and 1LBG (9).

Table 1. Repressor–Gold Nanocrystal Ratios (13.2 nm Gold Nanocrystals)^a

protein	repressors per nanocrystal		
	NaCl flocculation	[³⁵ S]-labeling	AU <i>S</i> _{max}
LacI	~12	7.1 ± 0.7	10.8 ± 0.7
T334C	~8	9.6 ± 0.2	10.4 ± 1.0.

^a For comparison, a theoretical prediction of 11 repressors per nanocrystal is based on the average diameter of the gold core from TEM data and dimensions from the LacI crystal structure 1LBI (9).

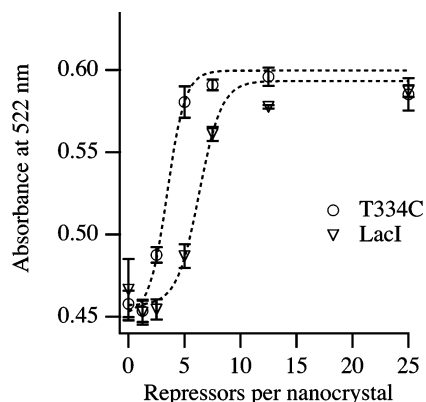


Figure 2. NaCl-induced flocculation of repressor conjugates. The absorbance of the gold nanocrystal plasmon peak was measured after NaCl was added to samples with a range of repressor concentrations. T334C (circles) prevents flocculation at lower concentration than LacI (triangles). Lines are shown for guidance only. Data are from three separate experiments.

gold–sulfur bond such as that engineered in T334C, native LacI repressors would require higher protein concentrations for stabilization.

The relative amount of gold nanocrystal and protein in these conjugates can also be found using radiolabeled [³⁵S]-repressor conjugates (Table 1). Here, [³⁵S]-repressors were conjugated to gold nanocrystals using our standard methods, and free protein was separated from conjugates by multiple rounds of centrifugation. The results show that LacI–gold nanocrystal conjugates have on average three fewer proteins per nanocrystal than conjugates produced using T334C mutants, a result that contradicts the trend found in the NaCl flocculation assay. In this analysis, bionanoconjugates were separated from proteins

using a strong centrifugal force (14000 rpm for 30 min) to rapidly pellet the sample; subsequent washes, and recovery, could result in the removal of weakly bound LacI repressor proteins from gold nanocrystal surfaces and subsequently lower [protein]/[nanocrystal] ratios. This effect would be less substantial for T334C–gold nanocrystal conjugates since conjugation in that case relies on the stronger gold–sulfur bond.

Bioconjugate structure can also be evaluated by shifts in the *S* value obtained from AU sedimentation velocity experiments (14). Sedimentation velocity, unlike repeated centrifugation and separation of pellet and supernatant, occurs at much lower centrifugal forces and in equilibrium (i.e., the components are not separated during the measurement). Therefore, the [gold nanocrystal]/[protein] values calculated using this technique should reflect both those protein molecules that are weakly and strongly bound to the nanocrystal surfaces. The ratios for both LacI and T334C proteins are ~10 repressors per nanocrystal. This result is consistent with the fact that, despite the mutation, LacI and T334C have the same physical dimensions. Given the average diameter of the gold nanocrystals used in these experiments (13.2 ± 1.5 nm) and the approximate dimensions of an unliganded LacI tetramer (7.8 × 7.9 × 7.7 nm) (9), we estimate 11 repressors as the maximum number that the surface of a gold nanocrystal could accommodate, in good agreement with our ratios as measured both by flocculation assays and in ultracentrifugation (Figure 3).

Of great interest in this work is how the conjugation process affects protein function, in this case the binding of operator DNA. To examine this, we used analytical ultracentrifugation to measure the sedimentation characteristics of conjugates mixed with operator DNA. When conjugated repressors interact with operator DNA, substantial changes in the hydrodynamic properties should be signaled by a change in the *S* values measured by AU. Figure 4 compares the *S* values of repressor conjugates with O¹ and an inducer sugar, IPTG. We first considered the properties of the native LacI conjugates. When the LacI conjugate is formed before O¹ is added, the nanocrystals have *S* values comparable to the LacI conjugate without O¹ (Figure 4A). This result suggests that O¹ is not binding to the conjugated LacI, as predicted if the nanocrystals are blocking the DNA recognition domain. We confirmed this by reversing the order of addition, and generated LacI–O¹ complexes that were then exposed to gold nanocrystals. These samples have higher *S*

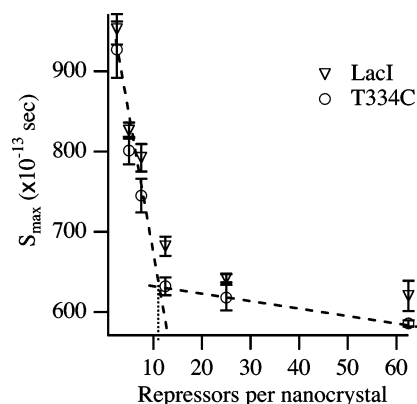


Figure 3. Repressor–gold nanocrystal stoichiometries using S_{\max} as an observable. The stoichiometric ratio corresponds to the point where the line fit at lower protein concentrations intersects the line extending the saturation plateau. For simplicity only the lines for LacI are shown. Both LacI (triangles) and T334C (circles) have similar ratios of ~ 10 repressors per nanocrystal ($D = 13.2$ nm) at the stoichiometric breakpoint. Data are from three separate experiments.

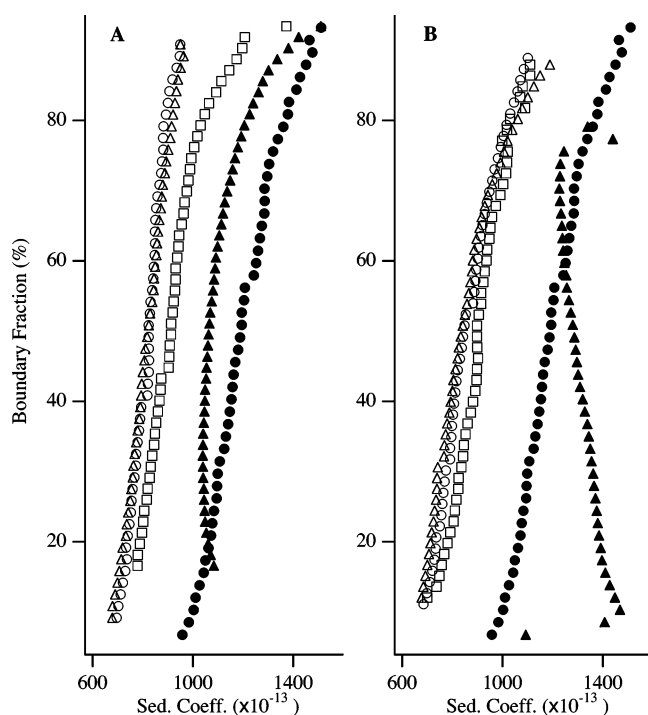


Figure 4. Comparison of S for repressor conjugates with O^1 and inducer IPTG. Integral plots from raw data analyzed in the Enhanced van Holde–Weischet utility in Ultrascan are shown. A, Samples containing LacI and B, samples containing T334C. ●, Gold nanocrystals (4 nM). △, Repressor (30 nM) gold nanocrystal (4 nM) conjugate. ○, Gold nanocrystal conjugated first, then operator (90 nM). ▲, Operator complexed first, then gold nanocrystals. □, Operator complexed first, then gold nanocrystals, then 1 mM IPTG. Data from three separate T334C–operator first experiments displayed a negative slope, indicative of strong repulsive interactions.

values comparable to gold nanocrystals alone, indicating no substantial conjugation occurs (Table 2). These data suggest that LacI interacts with either O^1 or gold nanocrystals, but does not significantly interact with both at the same time. In other words, the gold nanocrystals and operator DNA compete for the same binding site on the native LacI repressor.

The behavior of the mutant T334C repressor conjugates with operator DNA is quite different than that found for native LacI (Figure 4B). When the T334C conjugate is formed prior to O^1 addition, there is a small but significant increase in S (Table 2, $p < 0.2$). This change is larger than that for LacI under similar

Table 2. Average S Values of Repressor Conjugates with O^1 and IPTG

protein	AuNC	AuNC, then O^1	O^1 , then AuNC	O^1 , AuNC, then IPTG
LacI	838 \pm 9	855 \pm 21	1169 \pm 19	947 \pm 45
T334C	889 \pm 10	906 \pm 17	1242 \pm 69 ^a	952 \pm 56
no protein	1114 \pm 19	1147 \pm 11		1107 \pm 137

^a This value is not accurate due to the strong concentration-dependent nonideality in this sample (see Figure 4).

conditions. What remains uncertain is whether this change arises from conjugate–operator binding, or is the result of reduced nanocrystal coverage when T334C associates with O^1 instead of nonspecifically with the nanocrystal. Interestingly, when the T334C– O^1 complex is formed prior to conjugation, the data are poorly behaved in the van Holde–Weischet analysis and yield an S value distribution with a negative slope, indicative of repulsive interactions in the sample (Figure 4B). Second moment analysis of the data sets in Ultrascan reveal that there is a large concentration-dependent nonideality in these samples (not shown). One possible explanation for the concentration-dependent nonideality is that gold nanocrystals with a primary layer of T334C attached through the engineered cysteine and a secondary layer of O^1 bound to T334C have an exceptionally large hydrodynamic radius. If correct, these conjugates would also possess a strong negative charge on the surface. DNA and large particles like viral capsids are well-known for concentration-dependent nonideality, especially in the low salt conditions found in these experiments. The proposed O^1 –T334C–gold nanocrystal complex thus contains all of the elements that cause concentration-dependent nonideality in other systems. Interestingly, when IPTG is added to the T334C O^1 -first conjugates, the anomalous behavior is alleviated and the slope of the distribution becomes positive like the other samples. This result indirectly demonstrates that the nonideality is due to T334C– O^1 interactions, although confirmation of the assembly of the O^1 –T334C–gold nanocrystal complex cannot be unambiguously deduced from the sedimentation velocity experiments.

Although analytical ultracentrifugation indicates distinctive differences between how T334C and native LacI repressor conjugates recognize DNA, another method is required to confirm the relative ability of each system to interact with operator DNA. Electrophoretic mobility shift assays (EMSA) are readily adapted to this conjugate system. Indeed, agarose gel electrophoresis has been used previously to separate (18, 19), characterize the structure (20, 21), and quantify the binding (22) of gold nanocrystal–DNA conjugates. The assembly of albumin and antibody–quantum dot conjugates has also been assessed with polyacrylamide gel electrophoresis (23, 24). Here we use the EMSA to provide information about the operator DNA–repressor complexes.

An EMSA gel of repressor conjugates with [³²P]– O^1 is shown in Figure 5. The first four lanes establish the necessary controls. The faster migrating band present in the operator only control is attributed to single stranded DNA (lane 3). When O^1 is bound to unconjugated repressor, the free O^1 band is shifted due to a reduction in electrophoretic mobility (lanes 1 and 2), whereas gold nanocrystals alone do not cause a shift, establishing that there is no significant interaction between the operator and the nanocrystals (lane 4).

When the repressor–operator complex is formed before gold nanocrystals are added, native LacI retains significant O^1 binding affinity as an unconjugated protein, demonstrated by the band with similar mobility to the LacI–operator control (lanes 5–7). Here, the presence of operator appears to compete with conjugate formation, as observed in the AU experiments. Additional bands in these samples as compared to the control lanes are also apparent. First, the supershifted band (lowest mobility

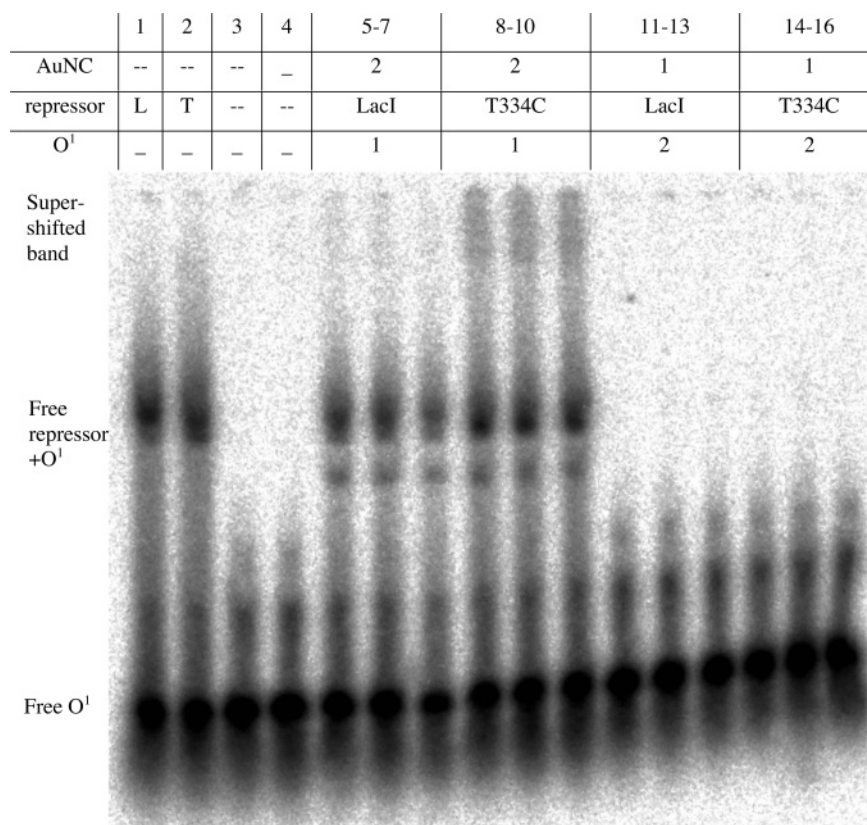


Figure 5. EMSA of 30 nM repressor conjugates with operator DNA O¹. [³²P]-O¹ (90 nM) is shown with 30 nM LacI (L) or T334C (T) and 4 nM gold nanocrystals. This protein concentration was chosen because it is slightly below the stoichiometric concentration for repressor–gold nanocrystal conjugation, so all of the protein should be conjugated in the gold nanocrystal-first conditions. The order of reaction components was varied and is denoted 1 or 2. Three predominant bands were observed corresponding to free O¹, unconjugated repressor–O¹ complex, and a super-shifted band representing O¹ bound to conjugate. Lanes 1–3, no nanocrystal added; 4, O¹ and nanocrystal; 5–7, LacI, O¹ added first; 8–10, T334C, O¹ first; 11–13, LacI, nanocrystal first; 14–16, T334C, nanocrystal first.

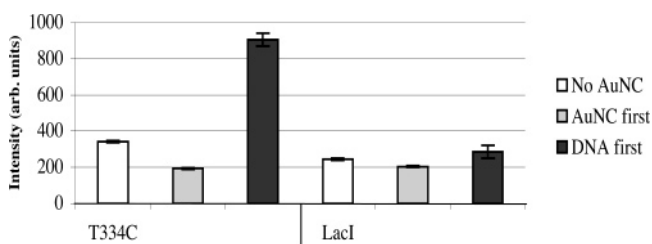


Figure 6. Quantification of the intensities of the supershifted bands in the EMSA. Intensities are measured in the region of the gel corresponding to the supershifted band. All areas used were identical, and data from three separate experiments were averaged. The T334C–O¹ first sample is the only one with significant intensity over background, demonstrating that T334C can interact with both O¹ and gold nanocrystal.

band), which we assign to O¹ bound to gold nanocrystal–protein conjugates (O¹•AuNC•protein) is more significant in the T334C sample (lanes 8–10) than for the native repressor, as predicted from the previous experiments. Visual inspection of the gel shows that, in addition to radiolabeled O¹, this region contains gold nanocrystal-based pink color (data not shown). Quantification of the [³²P]-O¹ signal from this band in Figure 6 shows that the T334C super-shifted band is ~3–4-fold more intense than the analogous LacI band, corresponding to enhanced DNA binding capacity of the T334C conjugate. This difference presumably arises from the ability of O¹-bound T334C to orient conjugation through the engineered cysteine sulfhydryl. The other observed band in lanes 5–10 not present in the control lanes is faster migrating and weaker in intensity than the unconjugated repressor–operator band; this band is assigned to two operators binding to a single tetramer. As expected, no

difference in the intensity of this band is observed between LacI and T334C.

In contrast, when LacI or T334C are conjugated to gold nanocrystals prior to the addition of O¹, signals are not observed at the positions corresponding to unconjugated repressor–O¹ complex nor the gold-nanocrystal-conjugated repressor–O¹ complex (lanes 11–16). At these repressor concentrations, little free protein appears to be present to form the unconjugated repressor–O¹ complex, and assembly of O¹-repressor–gold nanocrystal is precluded, presumably by gold nanocrystal binding blocking the basic DNA-binding domain. Note that conjugation prior to O¹ addition interferes with both LacI and T334C binding, suggesting that oriented binding by T334C does not preclude interaction of the basic N-terminal DNA binding domain with gold nanocrystals in the absence of operator DNA sequences.

Similar to AU, the EMSA data demonstrate that the order of addition of reactants is critical for the maintenance of DNA binding function, presumably due to an electrostatic interaction with the DNA-binding domain despite the strong nature of the possible T334C gold–sulfur bond. However, with addition of DNA first, T334C is able to conjugate to the gold nanocrystals through the engineered cysteine and retain significant interaction with O¹ as a conjugate.

DISCUSSION

We developed a LacI mutant designed with a solvent-exposed cysteine residue to facilitate directed conjugation through a gold–sulfur bond, alleviating the functionally deleterious consequences of nonspecific conjugation through the DNA-binding domain. This mutant, T334C, prevents NaCl-induced

flocculation at lower concentrations than native LacI. This observation suggests that LacI conjugates through a weaker, reversible electrostatic interaction, making it less efficient at preventing flocculation compared to T334C, which has the ability to conjugate through a gold–sulfur bond. Furthermore, more radiolabeled repressor is present in the T334C conjugate than the LacI conjugate after removal of free repressor via repeated centrifugation, indicating again that T334C has a stronger, more robust interaction with gold nanocrystals than LacI. Precise ratios of protein to nanocrystal were obtained under equilibrium conditions by the sedimentation velocity of conjugates. With this equilibrium technique, both LacI and T334C exhibit ratios of approximately 10 repressors per nanocrystal, in good agreement with calculations based on the nanocrystal and repressor dimensions.

Analytical ultracentrifugation and EMSA allow characterization of the interaction of conjugated LacI and T334C with the operator DNA sequence O¹. LacI conjugates do not interact strongly with O¹ in either assay. In contrast, T334C conjugates associate with O¹ depending on the order in which the operator–T334C–nanocrystal complex is formed. These data establish that T334C is capable of oriented conjugation to maintain DNA binding function, whereas LacI appears to conjugate primarily through its basic DNA-binding domain, thereby blocking the interaction with O¹ when conjugated. Nonspecific electrostatic protein–gold nanocrystal interactions, while easy to implement, may result in a loss of function for proteins with basic functional regions. If the biological function of the final hybrid material is to be maintained, the possibility of nonspecific interactions between functional regions and the nanostructure must be considered. We have shown that these complications can be avoided at least in part by directing conjugation using thiols placed in regions of the biomolecule that direct orientation to minimize inhibition of function.

ACKNOWLEDGMENT

The authors thank Jennifer Jamison for preparation of the gold nanocrystals used in this work and Joshua Falkner for TEM characterization of the nanocrystals. This work is supported in part by the Nanoscale Science and Engineering Initiative of the National Science Foundation under NSF Award Number EEC-0118007, The National Institutes of Health (GM22441), and the Robert A. Welch Foundation (C-576).

LITERATURE CITED

- (1) Keren, K., Krueger, M., Gilad, R., Ben-Yoseph, G., Sivan, U., and Braun, E. (2002) Sequence-specific molecular lithography on single DNA molecules. *Science* 297, 72–75.
- (2) Li, H., Park, S. H., Reif, J. H., LaBean, T. H., and Yan, H. (2004) DNA-templated self-assembly of protein and nanoparticle linear arrays. *J. Am. Chem. Soc.* 126, 418–419.
- (3) Pena, S. R. N., Raina, S., Goodrich, G. P., Fedoroff, N. V., and Keating, C. D. (2002) Hybridization and enzymatic extension of Au nanoparticle-bound oligonucleotides. *J. Am. Chem. Soc.* 124, 7314–7323.
- (4) Tsai, C.-Y., Shiao, A.-L., Cheng, P.-C., Shieh, D.-B., Chen, D.-H., Chou, C.-H., Yeh, C.-S., and Wu, C.-L. (2004) A Biological Strategy for Fabrication of Au/EGFP Nanoparticle Conjugates Retaining Bioactivity. *Nano Lett.* 4, 1209–1212.
- (5) Yun, C. S., Khitrov, G. A., Vergona, D. E., Reich, N. O., and Strouse, G. F. (2002) Enzymatic manipulation of DNA-nanomaterial constructs. *J. Am. Chem. Soc.* 124, 7644–7645.
- (6) Matthews, K. S., and Nichols, J. C. (1998) Lactose repressor protein: functional properties and structure. *Prog. Nuc. Acid Res. Mol. Biol.* 58, 127–164.
- (7) Zhou, D., Wang, X., Birch, L., Rayment, T., and Abell, C. (2003) AFM study on protein immobilization on charged surfaces at the nanoscale: Toward the fabrication of three-dimensional protein nanostructures. *Langmuir* 19, 10557–10562.
- (8) Brewer, S. H., Glomm, W. R., Johnson, M. C., Knag, M. K., and Franzen, S. (2005) Probing BSA binding to citrate-coated gold nanoparticles and surfaces. *Langmuir* 21, 9303–9307.
- (9) Lewis, M., Chang, G., Horton, N. C., Kercher, M. A., Pace, H. C., Schumacher, M. A., Brennan, R. G., and Lu, P. (1996) Crystal structure of the lactose operon repressor and its complexes with DNA and inducer. *Science* 271, 1247–1254.
- (10) Swint-Kruse, L., Elam, C. R., Lin, J. W., Wycuff, D. R., and Matthews, K. S. (2001) Plasticity of quaternary structure: Twenty-two ways to form a LacI dimer. *Protein Sci.* 10, 262–276.
- (11) Falcon, C. M., Swint-Kruse, L., and Matthews, K. S. (1997) Designed disulfide between N-terminal domains of lactose repressor disrupts allosteric linkage. *J. Biol. Chem.* 272, 26818–26821.
- (12) Falcon, C. M., and Matthews, K. S. (1999) Glycine insertion in the hinge region of lactose repressor protein alters DNA binding. *J. Biol. Chem.* 274, 30849–30857.
- (13) Chen, J., and Matthews, K. S. (1992) Deletion of lactose repressor carboxyl-terminal domain affects tetramer formation. *J. Biol. Chem.* 267, 13843–13850.
- (14) Calabretta, M., Jamison, J. A., Falkner, J. C., Liu, Y., Yuhas, B. D., Matthews, K. S., and Colvin, V. L. (2005) Analytical ultracentrifugation for characterizing nanocrystals and their bioconjugates. *Nano Lett.* 5, 963–967.
- (15) Wycuff, D. R., and Matthews, K. S. (2000) Generation of an AraC-araBAD promoter-regulated T7 expression system. *Anal. Biochem.* 277, 67–73.
- (16) Demeler, B. (2005) UltraScan 7.2. <http://www.ultrascan.uthscsa.edu/>.
- (17) Nakata, S., Kido, N., Hayashi, M., Hara, M., Sasabe, H., Sugawara, T., and Matsuda, T. (1996) Chemisorption of proteins and their thiol derivatives onto gold surfaces: Characterization based on electrochemical nonlinearity. *Biophys. Chem.* 62, 63–72.
- (18) Zanchet, D., Micheel, C. M., Parak, W. J., Gerion, D., and Alivisatos, A. P. (2001) Electrophoretic isolation of discrete Au nanocrystal/DNA conjugates. *Nano Lett.* 1, 32–35.
- (19) Arnaud, I., Abid, J.-P., Roussel, C., and Girault, H. H. (2005) Size-selective separation of gold nanoparticles using isoelectric focusing electrophoresis (IEF). *Chem. Commun.* 6, 787–788.
- (20) Parak, W. J., Pellegrino, T., Micheel, C. M., Gerion, D., Williams, S. C., and Alivisatos, A. P. (2003) Conformation of oligonucleotides attached to gold nanocrystals probed by gel electrophoresis. *Nano Lett.* 3, 33–36.
- (21) Zanchet, D., Micheel, C. M., Parak, W. J., Gerion, D., Williams, S. C., and Alivisatos, A. P. (2002) Electrophoretic and structural studies of DNA-directed Au nanoparticle groupings. *J. Phys. Chem. B* 106, 11758–11763.
- (22) Sandström, P., Boncheva, M., and Åkerman, B. (2003) Nonspecific and Thiol-Specific Binding of DNA to Gold Nanoparticles. *Langmuir* 19, 7537–7543.
- (23) Mamedova, N. N., Kotov, N. A., Rogach, A. L., and Studer, J. (2001) Albumin-CdTe nanoparticle bioconjugates: preparation, structure and interunit energy transfer with antenna effect. *Nano Lett.* 1, 281–286.
- (24) Wang, S., Mamedova, N., Kotov, N. A., Chen, W., and Studer, J. (2002) Antigen/antibody immunocomplex from CdTe nanoparticle bioconjugates. *Nano Lett.* 2, 817–822.

BC0600867